Journal of Computational Physics 229 (2010) 7806–7818

Contents lists available at ScienceDirect

Journal of Computational Physics

journal homepage: www.elsevier.com/locate/jcp

The momentum interpolation method based on the time-marching algorithm for All-Speed flows

Xue-song Li *, Chun-wei Gu

Key Laboratory for Thermal Science and Power Engineering of Ministry of Education, Department of Thermal Engineering, Tsinghua University, Beijing 100084, PR China

ARTICLE INFO

Article history:
Received 9 October 2009
Received in revised form 22 June 2010
Accepted 27 June 2010
Available online 1 July 2010

Keywords:
Time-marching algorithm
Momentum interpolation method
Checkerboard odd–even pressure–velocity decoupling
Preconditioning
Asymptotic analysis

ABSTRACT

The time-marching approach has clear physical meaning and strict mathematical nature and has been applied in computation of compressible flows widely and extended to many uniform algorithms for All-Speed flows. Remedy for its weakness in the problem of checkerboard decoupling of pressure field for incompressible flows is envisaged with the time-marching momentum interpolation method (MIM) taken into account in this paper. Existing preconditioning methods for suppressing decoupling and time-marching MIM are analyzed for this purpose, and algorithms of time-marching MIM are proposed for steady and unsteady flows and for All-Speed flows. Asymptotic analysis shows that the supposed time-marching MIM has at least a third-order accuracy, better than the existing time-marching coupling methods, which only have an accuracy of the same order as the adopted scheme has. Effects of the time step sizes on the ability of the time-marching MIM to suppress the checkerboard pressure decoupling are particularly discussed in terms of the dual-time stepping approach, and it is revealed how the decreased sizes of either the pseudo- or physical-time step increases the possibility of decoupling and how Choi's modification, in which the history of the interface velocity is decided by itself instead of the arithmetic average of the velocities on its adjacent nodes, removes the unphysical pressure oscillation with small size of the physical time step but leads to divergence with the pseudo-time step as well. As a remedy for the pseudo-time step, such methods are recommended as implicit methods and the local-time step method with a proposed modification of the time-marching MIM preventing accuracy loss due to very large time step size. Numerical experiments support the theoretical analyses and show the validity of the time-marching MIM proposed.

1. Introduction

The time-marching algorithm for temporal discretization is usually used in computation of compressible flows because of its clear physical meaning and strict mathematical nature, one of the most important advantages over computational methods for incompressible flows. Thus the time-marching algorithm has been extended to All-Speed flows including incompressible ones in such uniform methods as preconditioning methods [1–5] and All-Speed methods [6–8].

All those All-Speed methods, however, suffer from the classical problem of pressure–velocity decoupling, also known as checkerboard odd–even decoupling, in incompressible calculations. A few preconditioning methods, such as preconditioned Roe scheme [2] and preconditioned AUSMDV scheme [5], fortunately own an inherent mechanism to suppress checkerboard

* Corresponding author. Tel.: +86 10 62782907; fax: +86 10 62795946.
E-mail address: xs-li@mail.tsinghua.edu.cn (X.-s. Li).

0021-9991/$ - see front matter © 2010 Elsevier Inc. All rights reserved.
doi:10.1016/j.jcp.2010.06.039

decoupling [5,8]. Nevertheless, other original forms of preconditioned methods derived directly from the preconditioning rules, such as preconditioned AUSM+ scheme [5] and All-Speed methods [8], do not have such a mechanism. Therefore an additional measure, e.g. adding a first pressure-derivative smoothing term into the interface velocity as discussed in the Sections 2.3 and 2.4 or adopting staggered-grids or applying momentum interpolation in the collated grids, is needed to overcome the decoupling problem.

In solvers specially developed for incompressible flows such as SIMPLE-series algorithms, the staggered-grids method and the momentum interpolation method (MIM hereafter) are most used to suppress the checkerboard decoupling for a physical solution. Although the staggered-grids method is more effective, the MIM is preferred in practice because of its easier coding and less computational cost. The MIM was proposed firstly by Rhie and Chow [9], and has got great development for complex geometry [10], unsteady flows [11–14], flows with a large body force [15], etc.

For the time-matching preconditioning method, however, the general practice is adding a first pressure-derivative smoothing term into the interface mass flux or into the interface velocity [2,5–8,16] whether it is inherent or not, whereas the staggered-grids method or MIM is rarely seen in the literature.

The MIM interests us in understanding its relationship with the general preconditioning method and in integrating it with the time-marching algorithm to obtain an improved uniform method for All-Speed flows. An effort is accordingly tried in this work.

The outline of this paper is as follows. Section 2 gives the governing equations and briefly reviews the All-Speed method with a first pressure-derivative smoothing term in the interface velocity. Section 3 proposes versions of the MIM for steady, unsteady, and All-Speed calculations with the time-marching algorithm, and particularly discusses the effects of the time step. Section 4 makes an asymptotic analysis to demonstrate the behaviour of the time-marching MIM in the low Mach number limit, revealing its relationship with the method of adding the first pressure-derivative smoothing term. Section 5 gives some numerical experiments to support the theoretical analysis. Finally, Section 6 closes the paper with some concluding remarks.

2. The All-Speed method

2.1. Governing equations

For simplicity, the two-dimensional Euler compressible equations are written as

$$\frac{\partial \boldsymbol{Q}}{\partial t}+\frac{\partial \boldsymbol{F}}{\partial x}+\frac{\partial \boldsymbol{G}}{\partial y}=0, \tag{1}$$

where $\boldsymbol{Q}=\begin{bmatrix}\rho\\ \rho u\\ \rho v\\ \rho E\end{bmatrix}$ is the vector of conservation variables, $\boldsymbol{F}=\begin{bmatrix}\rho u\\ \rho u^2+p\\ \rho uv\\ u(\rho E+p)\end{bmatrix}$ and $\boldsymbol{G}=\begin{bmatrix}\rho v\\ \rho uv\\ \rho v^2+p\\ v(\rho E+p)\end{bmatrix}$ the vectors of Euler fluxes, ρ the fluid density, p the pressure, E the total energy, and u and v the velocity components in Cartesian coordinates (x, y), respectively.

For unsteady flows, the method of dual-time stepping is adopted in the next chapters and the governing equations should be rewritten correspondingly as follows:

$$\frac{\partial \boldsymbol{Q}}{\partial t}+\frac{\partial \boldsymbol{F}}{\partial x}+\frac{\partial \boldsymbol{G}}{\partial y}=-\frac{\partial \boldsymbol{Q}}{\partial \tau}, \tag{2}$$

where t is pseudo-time which marches in the inner layer of the iteration and τ is physical time which marches in the outer layer of the iteration.

Also for simplicity, in what follows discrete equations are given only for explicit schemes in one direction.

2.2. The general form of schemes and discussion on the dissipation terms

The numerical fluxes in many schemes can be expressed as the sum of the central terms $\widetilde{\boldsymbol{F}}_c$ and the numerical dissipation terms $\widetilde{\boldsymbol{F}}_d$:

$$\widetilde{\boldsymbol{F}}=\widetilde{\boldsymbol{F}}_c+\widetilde{\boldsymbol{F}}_d, \tag{3}$$

which is the general form of schemes.

Main idea of the All-Speed Roe method developed in Refs. [6–8] is to simply multiply the acoustic speed in eigenvalues of the present shock-capturing Roe scheme by a factor $f(M)$ to remedy its accuracy problems in the low Mach number limit, which is derived from the idea combining the Roe and Low-Speed-Roe [6] schemes with the function of local Mach number [7].

For the All-Speed Roe scheme, the numerical dissipation terms can be expressed as

$$\widetilde{\boldsymbol{F}}_{\boldsymbol{d},i+\frac{1}{2}j} = -\frac{1}{2}\boldsymbol{R}_{i+\frac{1}{2}j}\left|\boldsymbol{\Lambda}_{i+\frac{1}{2}j}\right|\boldsymbol{R}^{-1}_{i+\frac{1}{2}j}(\boldsymbol{Q}_{i+1,j}-\boldsymbol{Q}_{i,j}), \tag{4}$$

where $\boldsymbol{R}$ is the right eigenvector matrix of $\frac{\partial \boldsymbol{F}}{\partial \boldsymbol{Q}}$ and $\boldsymbol{\Lambda}$ the diagonal matrix formed with relevant pseudo-eigenvalues:

$$\lambda_{1,2} = u \quad \text{and} \quad \lambda_{3,4} = u \pm f(M)c. \tag{5}$$

And an expression of $f(M)$ is recommended as follows:

$$f(M) = \min\left(M\frac{\sqrt{4+(1-M^2)^2}}{1+M^2}, 1\right). \tag{6}$$

Compared with the traditional preconditioned Roe scheme, in which almost all terms of acoustic speed c are modified in both eigenvalues and corresponding eigenvector matrixes, the numerical dissipation terms Eq. (4) in the All-Speed Roe scheme only modifies the terms of c in the eigenvalues. Rationality of this procedure has been verified theoretically with an asymptotic analysis [8] and Hodge decomposition [17].

An advantage of the All-Speed Roe scheme is that it does not need the global cut-off strategy as required by the traditional preconditioned Roe scheme, because it removes the unstable structure $\frac{1}{f(M)c}$ that greatly magnifies the fluctuation of $f(M)c$ where its gradient is large as in the boundary layers [6]. Hence, All-Speed Roe scheme has better accuracy than the preconditioned Roe scheme theoretically, and the point is supported by numerical experiments [7]. In addition, Ref. [18] shows that the accuracy of the All-Speed Roe scheme is also better than those of the AUSM$^+$-up scheme and the SLAU scheme.

However, Eqs. (4)–(6) still suffer from the checkerboard decoupling for incompressible flows [7,8] although they are upwind-biased. Thus such additional procedures have to be introduced for a physical solution as adding a first pressure-derivative smoothing term, which will be discussed in the next section.

2.3. The central terms and the first pressure-derivative smoothing term

When the central terms are obtained by averaging the fluxes as:

$$\widetilde{\boldsymbol{F}}^{Roe}_{c,i+\frac{1}{2}j} = \frac{1}{2}\left(\overline{\boldsymbol{F}}_{i+\frac{1}{2}j,L} + \overline{\boldsymbol{F}}_{i+\frac{1}{2}j,R}\right), \tag{7}$$

the All-Speed Roe scheme, as mentioned above, suffers from the problem of checkerboard decoupling [7,8]. In order to obtain the physical pressure field, a pressure-dependent smoothing term, which is actually about the term of the first pressure derivative as discussed in Section 4, is added to the interface velocity in the central terms according to Refs. [5,16]:

$$\widetilde{\boldsymbol{F}}^{p}_{c,i+\frac{1}{2}j} = U_c\widehat{\boldsymbol{Q}}_{i+\frac{1}{2}j} + \boldsymbol{P}_{i+\frac{1}{2}j}, \tag{8}$$

where $U_c = \left(u_{i+\frac{1}{2}j,L} + u_{i+\frac{1}{2}j,R}\right)/2 - c_2/(\rho_0 u_0)\left(p_{i+\frac{1}{2}j,R} - p_{i+\frac{1}{2}j,L}\right)$, ρ_0 and u_0 mean reference density and velocity, respectively, $\widehat{\boldsymbol{Q}} = [\rho\ \rho u\ \rho v\ \rho E + p]^T$, and $\boldsymbol{P} = [0\ p\ 0\ 0]^T$.

2.4. Further analysis of the first pressure-derivative smoothing term

Eq. (8) provides an idea how to improve the preconditioned schemes without an inherent coupling mechanism.

In fact, some preconditioned schemes already have a similar inherent coupling mechanism. Ref. [5] gives such a classical example of AUSM-family schemes as follows.

The convective flux of AUSM-family schemes is defined as:

$$\boldsymbol{F}^c_{\frac{1}{2}} = (\rho u)_{\frac{1}{2}}\begin{bmatrix}1\\ u\\ v\\ H\end{bmatrix}_{i/i+1}.$$

The preconditioned AUSMDV scheme does have an inherent coupling mechanism because it inherently introduces the first pressure-derivative smoothing term $f(p_i - p_{i+1})$ into the interface mass flux as follows:

$$(\rho u)_{\frac{1}{2}} = \bar{a}_{\frac{1}{2}}\left\{\begin{array}{c}\rho_i\Pi^+_{(1)} + \rho_{i+1}\Pi^-_{(1)} + \\ \left(\Pi^+_{(4)} - \Pi^+_{(1)} + \Pi^-_{(4)} - \Pi^-_{(1)}\right)\frac{p_i+p_{i+1}}{p_i/\rho_i+p_{i+1}/\rho_{i+1}} + \\ \left(\Pi^+_{(4)} - \Pi^+_{(1)} - \Pi^-_{(4)} + \Pi^-_{(1)}\right)\frac{p_i-p_{i+1}}{p_i/\rho_i+p_{i+1}/\rho_{i+1}}\end{array}\right\},$$

where the first component is a simple advective upwind representation of the mass flux, the second component provides a stabilizing influence near sonic points, and the third is the pressure-dependent difference term that provides a global elliptic smoothing effect to suppress the decoupling tendency.

On the contrary, the original preconditioned AUSM+ scheme, which is also derived directly from the rules of preconditioning, does not contain a pressure-dependent smoothing term in the mass flux, so that it cannot prevent from the decoupling problem. To remedy this, a term behaving similarly to the pressure-smoothing component of the preconditioned AUSMDV scheme is added artificially into the mass flux for low-speed flows as:

$$(\rho u)_{\frac{1}{2}} = (\rho u)_{\frac{1}{2},\mathrm{AUSM}+} + \bar{a}_{\frac{1}{2}}\left(\frac{1}{(M_{ref})^2_{\frac{1}{2}} - 1}\right)\left\{\left(\Pi^+_{(4)} - \Pi^+_{(1)} - \Pi^-_{(4)} + \Pi^-_{(1)}\right)\frac{p_i - p_{i+1}}{p_i/\rho_i + p_{i+1}/\rho_{i+1}}\right\},$$

where $(\rho u)_{\frac{1}{2},\mathrm{AUSM}+}$ is the original AUSM+ interface flux. This artificial term will be turned off when the acoustic speed is reached.

It can be seen that the key to avoiding decoupling in preconditioned AUSM-family schemes is to add a first pressure-derivative smoothing term $f(p_i - p_{i+1})$ into the interface mass flux. In comparison, Eq. (8) is a simplified version, in which the term $f(p_i - p_{i+1})$ is introduced into the interface velocity with little variation of the density in the low Mach number limit taken into account.

Such an analysis can also be carried out for other schemes such as the preconditioned Roe scheme, in which the flux dissipation terms can be rearranged into the following form as in Ref. [2]:

$$\mathbf{\Gamma}|\boldsymbol{A}_\Gamma|\Delta\boldsymbol{Q} = |u|\begin{Bmatrix}\Delta(\rho)\\ \Delta(\rho v_x)\\ \Delta(\rho v_y)\\ \Delta(\rho v_z)\\ \Delta(\rho E)\end{Bmatrix}\boldsymbol{n} + \delta u\begin{Bmatrix}\rho\\ \rho v_x\\ \rho v_y\\ \rho v_z\\ \rho H\end{Bmatrix}\boldsymbol{n} + \delta p\begin{Bmatrix}0\\ \boldsymbol{i}\\ \boldsymbol{j}\\ \boldsymbol{k}\\ \boldsymbol{v}\end{Bmatrix},$$

where $\delta u = M^*\Delta u + [c^* - (1-2\alpha)|u| - \alpha u M^*]\frac{\Delta p}{\rho U_r^2}$, $\Delta\boldsymbol{Q} = \boldsymbol{Q}_R - \boldsymbol{Q}_L$, $\Delta u = \Delta\boldsymbol{v}\cdot\boldsymbol{n}$, $\delta p = M^*\Delta p + [c^* - |u| + \alpha u M^*]\rho\Delta u$, $c^* = \frac{|u'+c'|+|u'-c'|}{2}$, and $M^* = \frac{|u'+c'|-|u'-c'|}{2c'}$.

From this equation it is observed that a first pressure-derivative term $f(p_R - p_L)$ is contained in the term of δu that can be regarded as a part of the interface velocity. Thus, the preconditioned Roe scheme inherits the mechanism of Roe scheme to suppress decoupling. Asymptotic analysis [1,8] also confirms that Roe scheme and preconditioned Roe scheme satisfy homogeneous pressure Poisson-type equations for discrete governing equations to suppress decoupling. It is why very little discussion on decoupling is found in the references for these schemes.

The method with Eq. (8) is simple and effective for solving the decoupling problem, but an empirical constant c_2 has to be selected for specific problems, which is obviously undesirable for complex flows. Thus an improved method is needed.

As discussed in Section 1, the MIM is widely used in algorithms for incompressible flows. Because this method only modifies the central terms without involving the dissipation terms, it can be conveniently integrated into preconditioned or All-Speed schemes. Therefore, in Section 3 the MIM is improved for the time-marching algorithm and its relation with Eq. (8) is discussed.

3. The MIM for the time-marching algorithm

3.1. Governing equations

In the MIM, the concept of interface velocity is introduced and the governing equations (1) are rewritten as:

$$\frac{\partial\boldsymbol{Q}}{\partial t} + \frac{\partial\boldsymbol{F}^{\mathrm{MIM}}}{\partial x} + \frac{\partial\boldsymbol{G}^{\mathrm{MIM}}}{\partial y} = 0, \tag{9}$$

where $\boldsymbol{F}^{\mathrm{MIM}} = u_f\begin{bmatrix}\rho\\ \rho u\\ \rho v\\ \rho E + p\end{bmatrix} + \begin{bmatrix}0\\ p\\ 0\\ 0\end{bmatrix}$ and $\boldsymbol{G}^{\mathrm{MIM}} = v_f\begin{bmatrix}\rho\\ \rho u\\ \rho v\\ \rho E + p\end{bmatrix} + \begin{bmatrix}0\\ 0\\ p\\ 0\end{bmatrix}$, and u_f and v_f are components of the interface velocity, i.e. the velocity on the interface between adjacent control volumes. The key of the MIM is how to calculate the interface velocity.

When $u_f = U_c$, Eq. (9) is reduced to Eq. (8). As will be discussed in Chapter 4, Eq. (8) could be regarded as a coarser version of the MIM.

3.2. The MIM for single-time stepping method

For the control volume of a grid node (i,j), the following semi-discrete form of Eq. (9) can be obtained:

$$\frac{\partial\boldsymbol{Q}_{i,j}}{\partial t} = \Re_{i,j} = \Re^0_{i,j} - \begin{pmatrix}0 & \frac{\partial p}{\partial x} & \frac{\partial p}{\partial y} & 0\end{pmatrix}^T_{i,j}, \tag{10}$$

where $\Re_{i,j}$ is the spatial residual of Eq. (9) and $\Re^0_{i,j}$ is the residual excluding the pressure gradient.

For any grid node (i,j), the velocity at any position in the control volume can be calculated by the following equations:

$$(\rho u)_{i,j}^{n} = (\rho u)_{i,j}^{n-1} + \Delta t\left[\Re_{\rho u}^{0} - \frac{\partial p}{\partial x}\right]_{i,j}^{n-1}, \tag{11}$$

$$(\rho v)_{i,j}^{n} = (\rho v)_{i,j}^{n-1} + \Delta t\left[\Re_{\rho v}^{0} - \frac{\partial p}{\partial y}\right]_{i,j}^{n-1}. \tag{12}$$

So can the interface velocity components u_f and v_f. For the velocity on interface $(i+\frac{1}{2},j)$, the corresponding formulas are:

$$(\rho u_f)_{i+\frac{1}{2}j}^{n} = (\rho u)_{i+\frac{1}{2}j}^{n-1} + \Delta t\left[\Re_{\rho u}^{0} - \frac{\partial p}{\partial x}\right]_{i+\frac{1}{2}j}^{n-1}, \tag{13}$$

$$(\rho v_f)_{i+\frac{1}{2}j}^{n} = (\rho v)_{i+\frac{1}{2}j}^{n-1} + \Delta t\left[\Re_{\rho v}^{0} - \frac{\partial p}{\partial y}\right]_{i+\frac{1}{2}j}^{n-1}. \tag{14}$$

If all terms on the right side of Eqs. (13) and (14) are obtained by interpolation of values on the adjacent nodes, the interface velocity is actually the interpolated value of velocities on those nodes. For example, when the second-order central interpolation is used, the interface velocity components can be obtained as:

$$(u_f)_{i+\frac{1}{2}j}^{n} = 0.5\left(u_{i,j}^{n} + u_{i+1,j}^{n}\right), \tag{15}$$

$$(v_f)_{i+\frac{1}{2}j}^{n} = 0.5\left(v_{i,j}^{n} + v_{i+1,j}^{n}\right). \tag{16}$$

When Eqs. (15) and (16) are adopted, the corresponding fluxes defined in Eq. (9) will be very close to those in Eq. (7) in the low Mach number limit.

The key of the MIM is to determine pressure gradient $\left(\frac{\partial p}{\partial x}\right)_{i+\frac{1}{2}j}^{n-1}$ and $\left(\frac{\partial p}{\partial y}\right)_{i+\frac{1}{2}j}^{n-1}$ by calculation while to obtain other terms by interpolation. With this idea, Eqs. (13) and (14) can be expanded for the time-marching MIM as:

$$(u_f)_{i+\frac{1}{2}j}^{n} = \frac{1}{2}\left(u_{i,j}^{n-1} + u_{i+1,j}^{n-1}\right) + \Delta t\left[\frac{\left(\Re_{\rho u}^{0}\right)_{i,j}}{2\rho_{i,j}} + \frac{\left(\Re_{\rho u}^{0}\right)_{i+1,j}}{2\rho_{i+1,j}} - \frac{\left(\frac{\partial p}{\partial x}\right)_{i+1/2,j}}{\rho_{i+1/2,j}}\right]^{n-1}, \tag{17}$$

$$(v_f)_{i+\frac{1}{2}j}^{n} = \frac{1}{2}\left(v_{i,j}^{n-1} + v_{i+1,j}^{n-1}\right) + \Delta t\left[\frac{\left(\Re_{\rho v}^{0}\right)_{i,j}}{2\rho_{i,j}} + \frac{\left(\Re_{\rho v}^{0}\right)_{i+1,j}}{2\rho_{i+1,j}} - \frac{\left(\frac{\partial p}{\partial y}\right)_{i+1/2,j}}{\rho_{i+1/2,j}}\right]^{n-1}, \tag{18}$$

where the second-order central interpolation is applied to all terms except the pressure gradient.

With Eq. (10) and the assumption $\rho_{i,j}^{n} = \rho_{i,j}^{n-1}$ for low Mach numbers, Eqs. (17) and (18) can be rewritten as:

$$(u_f)_{i+\frac{1}{2}j}^{n} = 0.5\left(u_{i,j}^{n} + u_{i+1,j}^{n}\right) + \Delta t\left[\frac{\left(\frac{\partial p}{\partial x}\right)_{i,j}}{2\rho_{i,j}} + \frac{\left(\frac{\partial p}{\partial x}\right)_{i+1,j}}{2\rho_{i+1,j}} - \frac{\left(\frac{\partial p}{\partial x}\right)_{i+1/2,j}}{\rho_{i+1/2,j}}\right]^{n-1}, \tag{19}$$

$$(v_f)_{i+\frac{1}{2}j}^{n} = 0.5\left(v_{i,j}^{n} + v_{i+1,j}^{n}\right) + \Delta t\left[\frac{\left(\frac{\partial p}{\partial y}\right)_{i,j}}{2\rho_{i,j}} + \frac{\left(\frac{\partial p}{\partial y}\right)_{i+1,j}}{2\rho_{i+1,j}} - \frac{\left(\frac{\partial p}{\partial y}\right)_{i+1/2,j}}{\rho_{i+1/2,j}}\right]^{n-1}, \tag{20}$$

which are more convenient for analysis and coding than Eqs. (17) and (18) in many cases. Compared with Eqs. (15) and (16), Eqs. (19) and (20) include the additional pressure-dependent smoothing term, which is actually the third derivative of pressure under the assumption of constant density.

Pressure derivatives $\left(\frac{\partial p}{\partial x}\right)_{i+\frac{1}{2}j}^{n-1}$ and $\left(\frac{\partial p}{\partial y}\right)_{i+\frac{1}{2}j}^{n-1}$ are determined by calculation. For example, the simplest formulae are:

$$\left(\frac{\partial p}{\partial x}\right)_{i+1/2,j} = \frac{p_{i+1,j} - p_{i,j}}{\Delta x}, \tag{21}$$

$$\left(\frac{\partial p}{\partial y}\right)_{i+1/2,j} = \frac{p_{i+1/2,j+1/2} - p_{i+1/2,j-1/2}}{\Delta y}, \tag{22}$$

where $p_{i+1/2,j+1/2} = 0.25(p_{i,j} + p_{i+1,j} + p_{i,j+1} + p_{i+1,j+1})$, and

$$p_{i+1/2,j-1/2} = 0.25(p_{i,j} + p_{i+1,j} + p_{i,j-1} + p_{i+1,j-1}).$$

In order to obtain higher accuracy especially for complex grids and to avoid the pressure checkerboard effect, it is a better choice to utilize Gauss integral for calculation of the pressure gradient as follows:

$$\left(\frac{\partial p}{\partial x}\right)_{i+1/2,j} = \frac{1}{S_{i+1/2,j}} \oint pidl = \frac{p_{i+1,j}l_{x,2} - p_{i,j}l_{x,1} + p_{i+1/2,j+1/2}l_{x,4} - p_{i+1/2,j-1/2}l_{x,3}}{S_{i+1/2,j}},$$
$$\left(\frac{\partial p}{\partial y}\right)_{i+1/2,j} = \frac{1}{S_{i+1/2,j}} \oint pjdl = \frac{p_{i+1,j}l_{y,2} - p_{i,j}l_{y,1} + p_{i+1/2,j+1/2}l_{y,4} - p_{i+1/2,j-1/2}l_{y,3}}{S_{i+1/2,j}},$$

where $l_x = \boldsymbol{l}\cdot\boldsymbol{i}$, $l_y = \boldsymbol{l}\cdot\boldsymbol{j}$, $S_{i+1/2,j}$ is area of the surface enclosed by the dashed lines $\boldsymbol{l}$ (edges 1–4) in Fig. 1.

3.3. Discussion on effects of the time step size

For the original MIM [9], Refs. [11,12] point out that accuracy of the converged solution depends on the time step size and propose improvements. Ref. [13] further confirms that a checkerboard pressure field may occur again if the time step size is small and Choi's method proposed by Ref. [11] can be used to overcome this limit. Ref. [14] also discusses this problem and gives an improvement similar to Choi's method.

The time-marching MIM suffers from the same problems as the original MIM. It can be easily seen from Eqs. (19) and (20), in which the pressure-dependent smoothing term has the time step size Δt as its multiplying factor. Obviously, the converged interface velocity is dependent on Δt, and more seriously, the nonphysical oscillation in pressure field might occur when $\Delta t \to 0$ for the effect of the pressure-dependent smoothing term tends to vanish.

In order to overcome these limits, Choi [11] proposes that the history of the interface velocity is decided by itself instead of the arithmetic average of the velocities on its adjacent nodes. The same procedure is tried for the time-marching algorithm with terms $0.5\left(u_{ij}^{n-1} + u_{i+1j}^{n-1}\right)$ and $0.5\left(v_{ij}^{n-1} + v_{i+1j}^{n-1}\right)$ in Eqs. (17) and (18) replaced by $(u_f)_{i+\frac{1}{2}j}^{n-1}$ and $(v_f)_{i+\frac{1}{2}j}^{n-1}$, resulting in the following expressions:

$$(u_f)_{i+\frac{1}{2}j}^{n} = (u_f)_{i+\frac{1}{2}j}^{n-1} + \Delta t\left[\frac{\left(\Re_{\rho u}^{0}\right)_{i,j}}{2\rho_{i,j}} + \frac{\left(\Re_{\rho u}^{0}\right)_{i+1,j}}{2\rho_{i+1,j}} - \frac{\left(\frac{\partial p}{\partial x}\right)_{i+1/2,j}}{\rho_{i+1/2,j}}\right]^{n-1}, \tag{23}$$

$$(v_f)_{i+\frac{1}{2}j}^{n} = (v_f)_{i+\frac{1}{2}j}^{n-1} + \Delta t\left[\frac{\left(\Re_{\rho v}^{0}\right)_{i,j}}{2\rho_{i,j}} + \frac{\left(\Re_{\rho v}^{0}\right)_{i+1,j}}{2\rho_{i+1,j}} - \frac{\left(\frac{\partial p}{\partial y}\right)_{i+1/2,j}}{\rho_{i+1/2,j}}\right]^{n-1}. \tag{24}$$

Such a practice, however, leads to diverged results. This fact can be explained through a mathematic analysis. Approach of a stable converged solution of the interface velocity means that:

$$\Re_{i,j} = \Re_{i,j}^{0} - \left(0 \;\; \frac{\partial p}{\partial x} \;\; \frac{\partial p}{\partial y} \;\; 0\right)_{i,j}^{T} = 0,$$
$$(u_f)_{i+\frac{1}{2}j}^{n-1} = (u_f)_{i+\frac{1}{2}j}^{n}, \quad \text{and}$$
$$(v_f)_{i+\frac{1}{2}j}^{n-1} = (v_f)_{i+\frac{1}{2}j}^{n},$$

which are applied to Eqs. (23) and (24) to obtain the following necessary conditions for convergence:

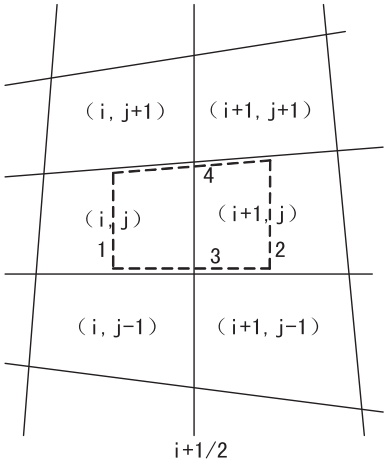

Fig. 1. Grids for Gauss integral.

$$\frac{\left(\frac{\partial p}{\partial x}\right)_{i,j}}{2\rho_{i,j}}+\frac{\left(\frac{\partial p}{\partial x}\right)_{i+1,j}}{2\rho_{i+1,j}}-\frac{\left(\frac{\partial p}{\partial x}\right)_{i+1/2,j}}{\rho_{i+1/2,j}}=0, \tag{25}$$

$$\frac{\left(\frac{\partial p}{\partial y}\right)_{i,j}}{2\rho_{i,j}}+\frac{\left(\frac{\partial p}{\partial y}\right)_{i+1,j}}{2\rho_{i+1,j}}-\frac{\left(\frac{\partial p}{\partial y}\right)_{i+1/2,j}}{\rho_{i+1/2,j}}=0. \tag{26}$$

Obviously it cannot be expected that those conditions are satisfied for most flow fields. Therefore, Eqs. (23) and (24) fail in the attempt to extend Choi's modification to the MIM for the time-marching algorithm.

Fortunately, various implicit methods of the time-marching algorithm may use remarkably increased time step sizes to smooth the pressure field although negative effects on accuracy of converged solution may occur as well. And many techniques for accelerating convergence while reaching the physical pressure field have been developed in calculation practice, such as the local-time step method, which increases the time step sizes for all grids except the smallest ones.

For accuracy of converged solution, however, a new question arises what happens to the new dissipation when Δt is very large rather than small. With a fully implicit method combined with Newton–Krylov or LU one can use a CFL (Courant–Priedrichs–Lewy) number of 1000 or above, similarly with the new acceleration scheme of Rossow [19]. Observing Eqs. (19) and (20), it seems that a dissipation that depends on Δt becomes too large and smears the entire solution and might even become unstable. In order to avoid this problem, the pressure derivatives $\left(\frac{\partial p}{\partial x}\right)^{n-1}_{i+\frac{1}{2}j}$ and $\left(\frac{\partial p}{\partial y}\right)^{n-1}_{i+\frac{1}{2}j}$ are redefined as follows:

$$\left(\frac{\partial p}{\partial x}\right)^{n-1}_{i+\frac{1}{2}j}=\beta\left[\left(\frac{\partial p}{\partial x}\right)^{n-1}_{i+\frac{1}{2}j}\right]_{calculation}+(1-\beta)\left[\left(\frac{\partial p}{\partial x}\right)^{n-1}_{i+\frac{1}{2}j}\right]_{interpolation}, \tag{27}$$

$$\left(\frac{\partial p}{\partial y}\right)^{n-1}_{i+\frac{1}{2}j}=\beta\left[\left(\frac{\partial p}{\partial y}\right)^{n-1}_{i+\frac{1}{2}j}\right]_{calculation}+(1-\beta)\left[\left(\frac{\partial p}{\partial y}\right)^{n-1}_{i+\frac{1}{2}j}\right]_{interpolation}, \tag{28}$$

where $0\leqslant\beta\leqslant 1$.

It means that the pressure derivatives are determined part by calculation and part by interpolation. Then, Eqs. (19) and (20) become

$$(u_f)^n_{i+\frac{1}{2}j}=0.5\left(u^n_{i,j}+u^n_{i+1,j}\right)+\beta\Delta t\left[\frac{\left(\frac{\partial p}{\partial x}\right)_{i,j}}{2\rho_{i,j}}+\frac{\left(\frac{\partial p}{\partial x}\right)_{i+1,j}}{2\rho_{i+1,j}}-\frac{\left(\frac{\partial p}{\partial x}\right)_{i+1/2,j}}{\rho_{i+1/2,j}}\right]^{n-1}, \tag{29}$$

$$(v_f)^n_{i+\frac{1}{2}j}=0.5\left(v^n_{i,j}+v^n_{i+1,j}\right)+\beta\Delta t\left[\frac{\left(\frac{\partial p}{\partial y}\right)_{i,j}}{2\rho_{i,j}}+\frac{\left(\frac{\partial p}{\partial y}\right)_{i+1,j}}{2\rho_{i+1,j}}-\frac{\left(\frac{\partial p}{\partial y}\right)_{i+1/2,j}}{\rho_{i+1/2,j}}\right]^{n-1}. \tag{30}$$

For convenience, above equations can be rewritten by redefining Δt in Eqs. (19) and (20):

$$\Delta t=\min(CFL,CFL_{min})\cdot\min\left(\frac{\Delta x}{u},\frac{\Delta y}{v}\right), \tag{31}$$

where CFL is CFL number determined by the implicit method, and CFL_{min} is minimum CFL number that can suppress checkerboard decoupling. Numerical experiments in the Section 5.1 show that CFL_{min} is of $O(1)$. Therefore, the negative effect on accuracy is limited within a reasonable bound for very large time step size due to implicit methods.

Another problem exists in the fact that the linear assumption, on which many usually used implicit methods like ADI-type and LU-type methods are based, makes a large time step size lose its physical meaning for time-accurate simulations. The local-time step method also suffers from this problem. Accordingly, the dual-time stepping approach is adopted and modified in the next section for the MIM for unsteady simulations.

3.4. The MIM with the dual-time stepping approach

The dual-time stepping approach is usually employed to obtained time-accurate solution with large time step sizes, especially for engineering calculations, and has been extended towards low-Mach-number flows [19,20]. With the MIM, the governing equations Eq. (2) for the dual-time stepping approach can be rewritten as:

$$\frac{\partial \boldsymbol{Q}}{\partial t}+\frac{\partial \boldsymbol{F}^{\mathrm{MIM}}}{\partial x}+\frac{\partial \boldsymbol{G}^{\mathrm{MIM}}}{\partial y}=-\frac{\partial \boldsymbol{Q}}{\partial \tau}, \tag{32}$$

where $\boldsymbol{Q}$, $\boldsymbol{F}^{\mathrm{MIM}}$ and $\boldsymbol{G}^{\mathrm{MIM}}$ have the same definitions as in Eq. (9), and t is the pseudo-time marched in inner layer of the iteration and τ the physical time marched in outer layer of the iteration. When $\Delta\tau\to\infty$, Eq. (32) becomes the single-time stepping Eq. (9). $\frac{\partial \boldsymbol{Q}}{\partial \tau}$ is treated as the source term and usually discretized by backward second-order difference as:

$$\frac{\partial \boldsymbol{Q}}{\partial \tau}=\frac{3\boldsymbol{Q}^k-4\boldsymbol{Q}^{k-1}+\boldsymbol{Q}^{k-2}}{2\Delta\tau}.$$

Without removing the effects of the time steps, the MIM based on the governing Eq. (32) are expressed as follows:

$$(u_f)^n_{i+\frac{1}{2}j} = 0.5\left(u^n_{ij} + u^n_{i+1j}\right) + \left(\frac{1}{\Delta t} + \frac{1.5}{\Delta \tau}\right)^{-1}\left[\frac{\left(\frac{\partial p}{\partial x}\right)_{ij}}{2\rho_{ij}} + \frac{\left(\frac{\partial p}{\partial x}\right)_{i+1j}}{2\rho_{i+1j}} - \frac{\left(\frac{\partial p}{\partial x}\right)_{i+1/2j}}{\rho_{i+1/2j}}\right]^{n-1}, \tag{33}$$

$$(v_f)^n_{i+\frac{1}{2}j} = 0.5\left(v^n_{ij} + v^n_{i+1j}\right) + \left(\frac{1}{\Delta t} + \frac{1.5}{\Delta \tau}\right)^{-1}\left[\frac{\left(\frac{\partial p}{\partial y}\right)_{ij}}{2\rho_{ij}} + \frac{\left(\frac{\partial p}{\partial y}\right)_{i+1j}}{2\rho_{i+1j}} - \frac{\left(\frac{\partial p}{\partial y}\right)_{i+1/2j}}{\rho_{i+1/2j}}\right]^{n-1}. \tag{34}$$

Sizes of both pseudo-time step size Δt and physical time step size $\Delta \tau$ have effects on the MIM as shown in Eqs. (33) and (34). It will lose efficiency if the size of any time steps becomes too small. The pseudo-time step size Δt can be increased in implicit methods and the local-time step method, but the physical time step size $\Delta \tau$ has to be decided by physical requirements. Fortunately, although Choi's method cannot be applied to the pseudo-time step as discussed in Section 3.3, it is effective for the physical time step and the correspondingly modified MIM are expressed as follows:

$$\begin{aligned}(u_f)^n_{i+\frac{1}{2}j} = {} & 0.5\left(u^n_{ij} + u^n_{i+1j}\right) + \left(\frac{1}{\Delta t} + \frac{1.5}{\Delta \tau}\right)^{-1}\left[\frac{\left(\frac{\partial p}{\partial x}\right)_{ij}}{2\rho_{ij}} + \frac{\left(\frac{\partial p}{\partial x}\right)_{i+1j}}{2\rho_{i+1j}} - \frac{\left(\frac{\partial p}{\partial x}\right)_{i+1/2j}}{\rho_{i+1/2j}}\right]^{n-1} \\ & + \left(\frac{1}{\Delta t} + \frac{1.5}{\Delta \tau}\right)^{-1}\left[\frac{-4u^{k-1}_{ij} + u^{k-2}_{ij} - 4u^{k-1}_{i+1j} + u^{k-2}_{i+1j}}{4\Delta\tau} - \frac{-4(u_f)^{k-1}_{i+\frac{1}{2}j} + (u_f)^{k-2}_{i+\frac{1}{2}j}}{2\Delta\tau}\right],\end{aligned} \tag{35}$$

$$\begin{aligned}(v_f)^n_{i+\frac{1}{2}j} = {} & 0.5\left(v^n_{ij} + v^n_{i+1j}\right) + \left(\frac{1}{\Delta t} + \frac{1.5}{\Delta \tau}\right)^{-1}\left[\frac{\left(\frac{\partial p}{\partial y}\right)_{ij}}{2\rho_{ij}} + \frac{\left(\frac{\partial p}{\partial y}\right)_{i+1j}}{2\rho_{i+1j}} - \frac{\left(\frac{\partial p}{\partial y}\right)_{i+1/2j}}{\rho_{i+1/2j}}\right]^{n-1} \\ & + \left(\frac{1}{\Delta t} + \frac{1.5}{\Delta \tau}\right)^{-1}\left[\frac{-4v^{k-1}_{ij} + v^{k-2}_{ij} - 4v^{k-1}_{i+1j} + v^{k-2}_{i+1j}}{4\Delta\tau} - \frac{-4(v_f)^{k-1}_{i+\frac{1}{2}j} + (v_f)^{k-2}_{i+\frac{1}{2}j}}{2\Delta\tau}\right],\end{aligned} \tag{36}$$

where the superscripts k and n are the iterative numbers of the physical time and pseudo-time, respectively. When n becomes large enough, $\phi^n = \phi^k$.

So Eqs. (35) and (36) are the proposed time-marching MIM for unsteady simulations. It can also be formally used for steady simulations provided that both the physical time step size $\Delta \tau$ and inner iteration number n are set to a very large number, e.g. 10^{30}, with which Eqs. (35) and (36) would be reduced to Eqs. (19) and (20).

3.5. The time-marching MIM for All-Speed flows

According to the interface velocity obtained from Eqs. (35) and (36), the central terms of the time-marching MIM are given as follows:

$$\widetilde{\boldsymbol{F}}^{\mathrm{MIM}}_{c,i+\frac{1}{2}} = \frac{1}{2}(u_f)_{i+\frac{1}{2}}\begin{bmatrix}\rho_L + \rho_R \\ (\rho u)_L + (\rho u)_R \\ (\rho v)_L + (\rho v)_R \\ (\rho E + p)_L + (\rho E + p)_R\end{bmatrix} + \frac{1}{2}\begin{bmatrix}0 \\ (p)_L + (p)_R \\ 0 \\ 0\end{bmatrix}. \tag{37}$$

Upon considering that the MIM is undesirable and should be turned off for high-Mach-number flows, the central terms for All-Speed flows can be expressed as combination of Eqs. (37) and (7) with the function $f(M)$ shown in Eq. (6) as the factor:

$$\widetilde{\boldsymbol{F}}_{c,i+\frac{1}{2}} = f(M)\widetilde{\boldsymbol{F}}^{Roe}_{c,i+\frac{1}{2}} + [1 - f(M)]\widetilde{\boldsymbol{F}}^{\mathrm{MIM}}_{c,i+\frac{1}{2}}. \tag{38}$$

Consequently, the required uniform algorithm for All-Speed flows are composed of the central terms Eq. (38) and the numerical dissipation terms Eq. (4).

3.6. The time-marching MIM for complex geometries

For complex geometries, Eq. (37) can be rewritten as follows:

$$\widetilde{\boldsymbol{F}}^{\mathrm{MIM}}_{c,i+\frac{1}{2}} = \frac{1}{2}(U_f)_{i+\frac{1}{2}}\begin{bmatrix}\rho_L + \rho_R \\ (\rho u)_L + (\rho u)_R \\ (\rho v)_L + (\rho v)_R \\ (\rho E + p)_L + (\rho E + p)_R\end{bmatrix} + \frac{1}{2}\begin{bmatrix}0 \\ (p)_L + (p)_R \\ 0 \\ 0\end{bmatrix}, \tag{39}$$

where $U_f = \xi_x u_f + \xi_y v_f$, ξ_x, ξ_y are transformation coefficients of the grid systems, and u_f and v_f are determined by Eqs. (35) and (36), respectively.

4. Asymptotic analysis

Asymptotic analysis is usually utilized to research the behaviour of continuous or discrete flows in the low Mach number limit [1,8,21–23]. For analyzing a steady low-Mach-number flow, all non-dimensional variables are asymptotically expanded into powers of the reference Mach number M^*:

$$\tilde{\phi} = \tilde{\phi}^0 + M_* \tilde{\phi}^1 + M_*^2 \tilde{\phi}^2 + M_*^3 \tilde{\phi}^3 + \cdots,$$

where ϕ represents each of the fluid variables, i.e. ρ, u, v, E, or p.

For governing equations (1) for a continuous case, the velocity field is subject to a divergence constraint as the Mach number diminishes to zero:

$$\mathrm{div}(\boldsymbol{u}^0) = 0. \tag{40}$$

While in a discrete case the velocity field, as proved in Ref. [8], has such a feature as:

$$u^0_{i+1,j} - u^0_{i-1,j} + v^0_{i,j+1} - v^0_{i,j-1} = 0, \tag{41}$$

provided that uniform Cartesian meshes and the Low-Speed-Roe or All-Speed-Roe scheme are used with the central terms in the form of Eq. (7).

That is to say, the All-Speed-Roe scheme has the same behaviour in the low Mach number limit as the original governing equations for a continuous case. Meanwhile, Ref. [8] also demonstrates that the All-Speed-Roe scheme does not have an inherent mechanism to suppress the checkerboard decoupling.

For the traditional preconditioned Roe scheme, the behaviour of the discrete velocity field is shown as follows:

$$u^0_{i+1,j} - u^0_{i-1,j} + v^0_{i,j+1} - v^0_{i,j-1} = -\frac{1}{\rho^0_l E^0_l + p^0_l} \sum_{l \in v(i)} \frac{h^0_{il}}{2\sqrt{Y^0_{il}}} U^0_{il} \rho^0_{il} \Delta_{il} U^0 + \frac{h^0_{il}}{\sqrt{Y^0_{il}}} \Delta_{il} p^2 \neq 0, \tag{42}$$

which means that so discretized velocity field does not satisfy the zero Mach number divergence constraint as Eq. (40). However, this scheme possesses an inherent mechanism to remove the unrealistic pressure field effectively as discussed in Section 2.4.

For the All-Speed-Roe scheme, when Eq. (8) is used, in which a first pressure-derivative smoothing term is added into the interface velocity, a mechanism is also provided to suppress the checkerboard mode just like in the traditional preconditioned Roe scheme [8]. But unfortunately, Eq. (8) also leads to non-zero velocity divergence:

$$u^0_{i+1,j} - u^0_{i-1,j} + v^0_{i,j+1} - v^0_{i,j-1} = c_2 \left(p^2_{i+1,j} + p^2_{i-1,j} + p^2_{i,j+1} + p^2_{i,j-1} - 4p^2_{i,j} \right) = c_2 (\Delta x)^2 \nabla^2 p^2. \tag{43}$$

For the time-marching MIM such as Eqs. (19) and (20), with

$$\frac{1}{2}\left(\frac{\partial p}{\partial x}\right)_{i,j} + \frac{1}{2}\left(\frac{\partial p}{\partial x}\right)_{i+1,j} - \left(\frac{\partial p}{\partial x}\right)_{i+1/2,j} = \frac{1}{4}(\Delta x)^2 \left(\frac{\partial^3 p}{\partial x^3}\right)_{i+1/2,j}, \tag{44}$$

$$\frac{1}{2}\left(\frac{\partial p}{\partial y}\right)_{i,j} + \frac{1}{2}\left(\frac{\partial p}{\partial y}\right)_{i,j+1} - \left(\frac{\partial p}{\partial y}\right)_{i,j+1/2} = \frac{1}{4}(\Delta x)^2 \left(\frac{\partial^3 p}{\partial y^3}\right)_{i,j+1/2}, \tag{45}$$

and the local pseudo-time decided by CFL condition as

$$\Delta t = CFL \cdot \min\left(\frac{\Delta x}{u}, \frac{\Delta y}{v}\right) = CFL \cdot \frac{\Delta x}{u} \quad \text{if } u \geqslant v, \tag{46}$$

where CFL is CFL number, it is follows that

$$u^0_{i+1,j} - u^0_{i-1,j} + v^0_{i,j+1} - v^0_{i,j-1} = \frac{CFL}{\rho^0 u^0} (\Delta x)^4 \nabla^4 p^2. \tag{47}$$

In comparison, the All-Speed-Roe scheme with Eq. (8), in which the first pressure derivative is introduced into the interface velocity, has a global second-pressure-derivative smoothing effect for the discrete governing equations as shown in Eq. (43), while the time-marching MIM Eqs. (19) and (20), in which the third pressure derivative is introduced as indicated by Eqs. (44) and (45), has a global fourth-pressure-derivative smoothing effect as shown in Eq. (47).

As to the cost for preventing the checkerboard decoupling, Eqs. (43) and (47) show that both methods do not satisfy zero velocity divergence condition strictly. However, the former introduces into $\mathrm{div}(\boldsymbol{u}^0)$ a spatially first-order numerical error scaled to Δx as seen from Eq. (43). Instead, the latter introduces a spatially third-order error scaled to Δx^3 as seen from Eq. (47). Therefore, from the numerical viewpoint, the time-marching MIM proposed in the paper will actually satisfy zero

velocity divergence condition if popular second-order schemes are used. On the contrary, the error caused by the All-Speed-Roe scheme with Eq. (8) cannot be ignored.

It should be noticed that this analysis is based on the first-order scheme and the first-order pressure difference $p_{i+1} - p_i$ in Eq. (8). If $p_{i+1} - p_i$ is replaced by a higher order pressure difference $p_R - p_L$ with the scheme reconstructed the same way, the smoothing term will introduce the similarly higher order errors. Therefore, strictly speaking, Eq. (8) produces the same order numerical errors as the order of the scheme and still cannot be ignored. On the contrary, Eqs. (19) and (20) produce at least third-order numerical errors, which can be ignored for the second-order schemes usually used for the finite volume method, and can provide even higher order accuracy with higher order discretization of the interface pressure gradient.

According to the aforementioned discussions, Eq. (8) can be regarded as a coarser version of the time-marching MIM for the similar mechanism of introducing pressure derivatives into the interface velocity and its lower order numerical errors.

5. Numerical experiments

In order to examine the features of the proposed time-marching MIM, the flow past a high-load turbine blade (T106) row is simulated at inlet Mach number 0.001. The numerical dissipation terms are adopted from Eqs. (4)–(6) of the All-Speed Roe scheme, and MUSCL reconstruction is applied for a second-order accuracy. The DP-LUR implicit method [24] with preconditioning modification for low-Mach-number flows and the local-time step method are utilized to accelerate convergence and to help pressure–velocity coupling.

5.1. Steady simulation for inviscid flow

The steady inviscid solution of T106 blade row is obtained through the single-time stepping method with 40×98 grid points in azimuthal and streamwise directions. When the interface velocity is determined by central interpolation as Eqs. (15) and (16), the pressure field suffers from serious checkerboard decoupling as shown in Fig. 2. When Eqs. (19) and (20) of the time-marching MIM are adopted and CFL number is equal to 0.01, the oscillation of the pressure field is also obvious although great improvement has been gained as shown in Fig. 3. Increasing CFL number to 2 completely removes the oscillation of the pressure field as shown in Fig. 4. Therefore, Eqs. (19) and (20) of the time-marching MIM are effective for avoiding unphysical solutions, but the effects are really influenced by the size of the time step. If Choi's modification as shown in Eqs. (23) and (24) is used, the computation diverges very soon even the physical solution in Fig. 4 is used as

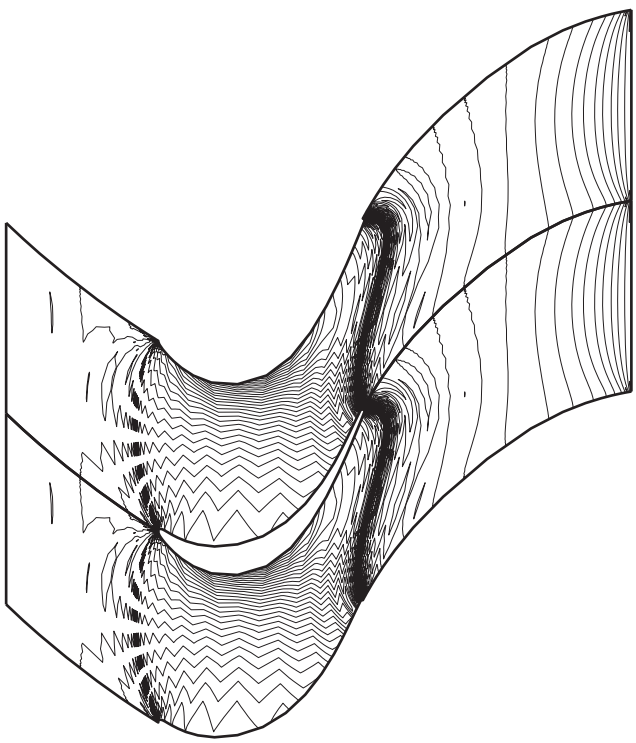

Fig. 2. Pressure contours with full decoupling.

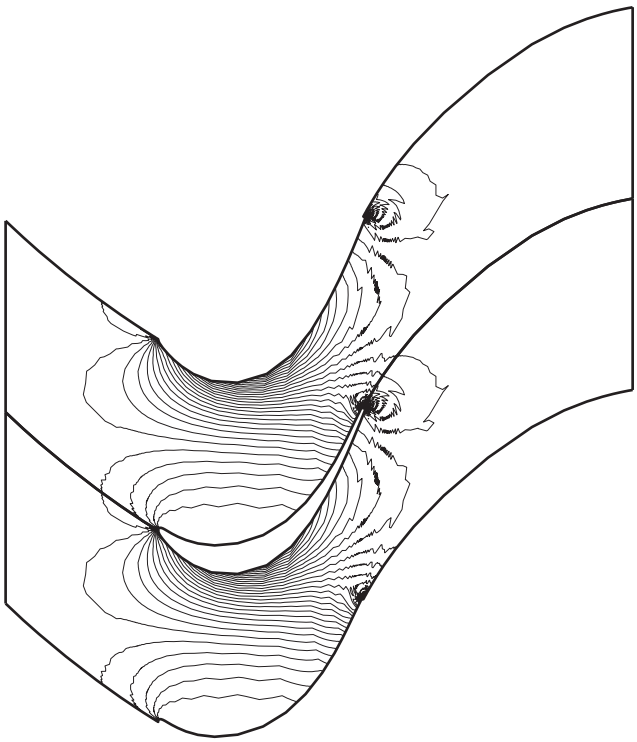

Fig. 3. Pressure contours with partial decoupling.

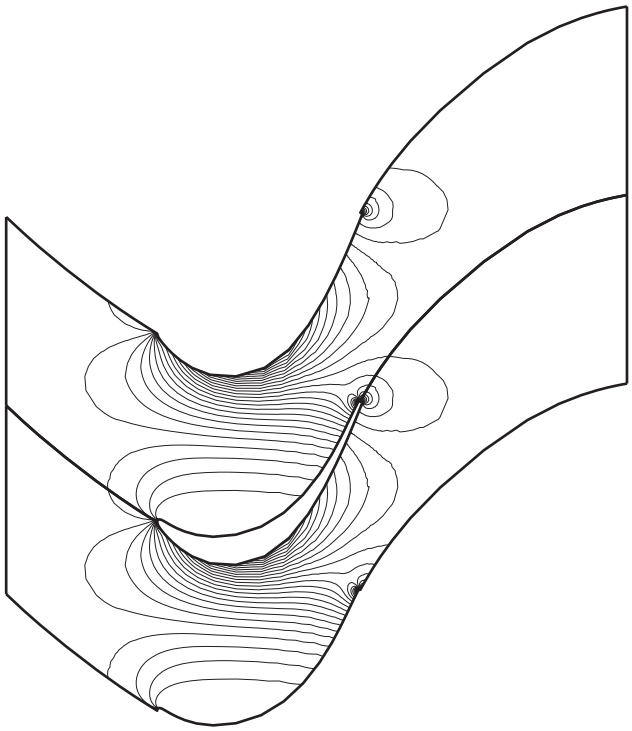

Fig. 4. Pressure contours of physical solution.

the initial field. Fortunately, a CFL number of $O(1)$ is good enough for physical solutions, and thus it is not a rigorous limitation to the time-marching MIM.

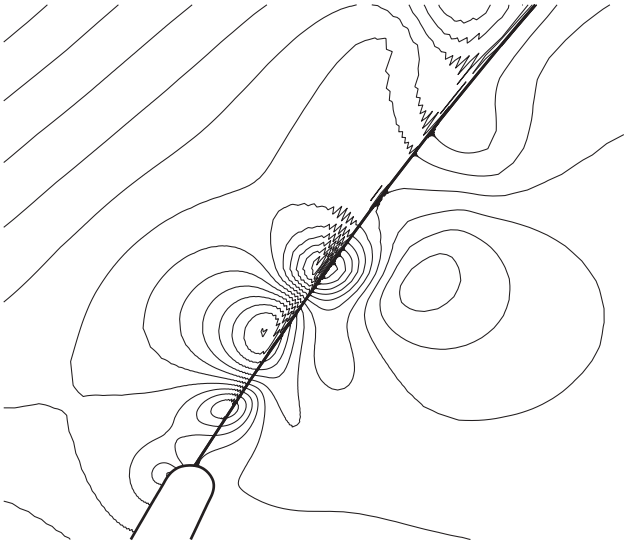

Fig. 5. Instantaneous results with Eqs. (33) and (34).

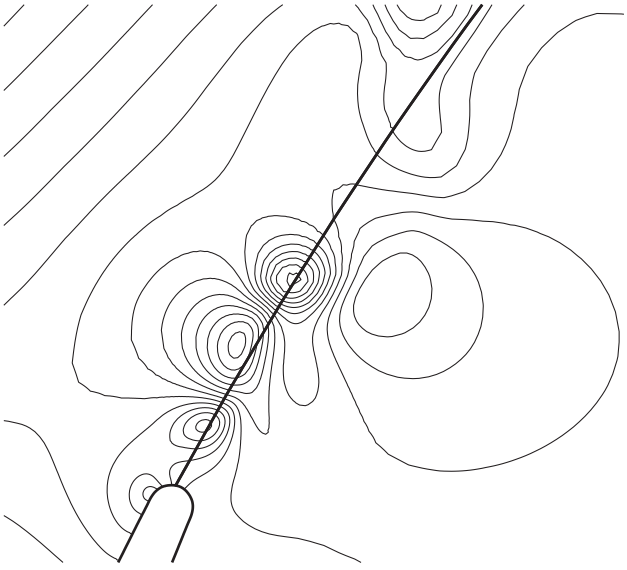

Fig. 6. Instantaneous results with Eqs. (35) and (36).

5.2. Unsteady simulation at Reynolds number 5000

In order to validate the necessity of including terms of the physical time derivatives in Eqs. (35) and (36) for time-accurate solution, a large eddy simulation is carried out for the unsteady flow past T106 blade row at Reynolds number 5000 with 128×680 grid points, numerical CFL number 2, and physical time step $\Delta\tau = 3\times10^{-6}$. After 50,000 physical time steps, the periodic solution is reached. Figs. 5 and 6 give the instantaneous pressure contours by different schemes from the same initial condition after the same number of physical time steps. The results by Eqs. (33) and (34) in Fig. 5 suffer from obvious checkerboard decoupling especially in the wake due to the small size of the physical time step, while the results by Eqs. (35) and (36) in Fig. 6 show no such problem.

6. Conclusions

In this paper, the MIM is discussed in the frame of the time-marching approach, the time-marching algorithms with MIM are proposed for steady and unsteady flows based on single- and dual-time stepping respectively, and the time-marching

MIM is applied to a unified algorithm for compressible and incompressible flows. Similar to the traditional preconditioning time-marching algorithms proposed by previous authors [2,5,16], the time-marching MIM introduces a pressure derivative into the interface velocity. The improvement lies in the fact that the time-marching MIM introduces the third pressure derivative, which leads to at least the third-order accuracy, while the traditional preconditioning methods can only reach an accuracy the same order as the scheme adopted.

As to the dual-time stepping approach applied to the proposed time-marching algorithms, an analysis is made to identify the effects of both the pseudo- and physical-time step sizes on pressure oscillation and on convergence of the solution. It is proved that Choi's modification for pseudo-time step size fails here for leading to divergence, and that only such methods that increase the size of the pseudo-time step as implicit methods and local-time step method can be adopted for assuring physical solutions with a proposed modification preventing loss of accuracy due to very large time step size of implicit methods. However, Choi's modification is still effective for the physical time step size and can be so applied to make the time-marching algorithms adaptive for unsteady simulations. Numerical experiments are carried out to validate the analysis, showing that the time-marching algorithms proposed in this paper are well able to suppress the checkerboard decoupling of the pressure field for both steady and unsteady flows.

Acknowledgments

This work is supported by Project 50806037 of National Natural Science Foundation of China and Project 2007CB210105 of 973 Program. We also thank Prof. Wang Cuncheng for polishing the paper.

References

[1] H. Guillard, C. Viozat, On the behaviour of upwind schemes in the low Mach number limit, Computers and Fluids 28 (1999) 63–86.
[2] J.M. Weiss, W.A. Smith, Preconditioning applied to variable and const. density flows, AIAA Journal 33 (1995) 2050–2057.
[3] E. Turkel, Preconditioned methods for solving the incompressible and low speed compressible equations, Journal of Computational Physics 72 (1987) 277–298.
[4] E. Turkel, Preconditioning techniques in computational fluid dynamics, Annual Reviews of Fluid Mechanics 31 (1999) 385–416.
[5] J.R. Edwards, M.S. Liou, Low-diffusion flux-splitting methods for flows at all speeds, AIAA Journal 36 (1998) 1610–1617.
[6] X.S. Li, J.Z. Xu, C.W. Gu, Preconditioning method and engineering application of large eddy simulation, Science in China Series G: Physics, Mechanics & Astronomy 51 (2008) 667–677.
[7] X.S. Li, C.W. Gu, J.Z. Xu, Development of Roe-Type Scheme for All-Speed flows based on preconditioning method, Computers and Fluids 38 (2009) 810–817.
[8] X.S. Li, C.W. Gu, An All-Speed Roe-Type Scheme and its asymptotic analysis of low-Mach-number behaviour, Journal of Computational Physics 227 (2008) 5144–5159.
[9] C.M. Rhie, W.L. Chow, Numerical study of the turbulent flow past an airfoil with trailing edge separation, AIAA Journal 21 (1983) 1525–1532.
[10] S.K. Choi, H.Y. Nam, M. Cho, Use of the momentum interpolation method for numerical solution of incompressible flows in complex geometries: choosing cell face velocities, Numerical Heat Transfer, Part B: Fundamentals 23 (1993) 21–41.
[11] S.K. Choi, Note on the use of momentum interpolation method for unsteady flows, Numerical Heat Transfer, Part A: Applications 36 (1999) 545–550.
[12] B. Yu, W.Q. Tao, J.J. Wei, et al, Discussion on momentum interpolation method for collocated grids of incompressible flow, Numerical Heat Transfer, Part B: Fundamentals 42 (2002) 141–166.
[13] B. Yu, Y. Kawaguchi, W.Q. Tao, et al, Checkerboard pressure predictions due to the underrelaxation factor and time step size for a nonstaggered grid with momentum interpolation method, Numerical Heat Transfer, Part B: Fundamentals 41 (2002) 85–94.
[14] W.Z. Shen, J.A. Michelsen, J.N. Sorensen, Improved Rhie–Chow interpolation for unsteady flow computations, AIAA Journal 39 (2001) 2406–2409.
[15] S.K. Choi, Use of the momentum interpolation method for flows with a large body force, Numerical Heat Transfer, Part B: Fundamentals 43 (2003) 267–287.
[16] I. Mary, P. Sagaut, Large eddy simulation of flow around an airfoil near stall, AIAA Journal 40 (2002) 1139–1145.
[17] S. Dellacherie, Analysis of Godunov type schemes applied to the compressible Euler system at low Mach number, Journal of Computational Physics 229 (2010) 978–1016.
[18] K. Kitamura, K. Fujimoto, E. Shima, Performance of Low-Dissipation Euler Fluxes and Preconditioned Implicit Schemes in Low Speeds, AIAA Paper 2010-1272.
[19] C.C. Rossow, Efficient computation of compressible and incompressible flows, Journal of Computational Physics 220 (2007) 879–899.
[20] E. Turkel, V.N. Vatsa, Local preconditioners for steady and unsteady flow applications, Mathematical Modelling and Numerical Analysis 39 (2005) 515–535.
[21] S. Klainerman, A. Majda, Compressible and incompressible fluids, Communications on Pure Applied Mathematics 35 (1982) 629–651.
[22] R. Klein, Semi-implicit extension of a Godunov-type scheme based on low Mach number asymptotics I: One-dimensional flow, Journal of Computational Physics 121 (1995) 213–237.
[23] A. Meister, Asymptotic based preconditioning technique for low Mach number flows, Zeitschrift Fur Angewandte Mathematik Und Mechanik 83 (2003) 3–25.
[24] M.J. Wright, G.V. Candler, Prampolini M. Data-Parallel, Lower-upper relaxation method for the Navier–Stokes equations, AIAA Journal 34 (1996) 1371–1377.